Supporting Information for

A porous anionic zinc(II) metal-organic framework for gas adsorption, selective uptake of dyes and sensing of Fe^{3+} by Tb^{3+} ion encapsulation

Yu-Jie Liang,‡ Jun Yao,‡ Min Deng, Yan-E Liu, Quan-Qing Xu, Qiu-Xia Li, Bi Jing, Ai-Xin Zhu* and

Bo Huang*

Faculty of Chemistry and Chemical Engineering, Yunnan Normal University, Kunming 650500, China.

E-mail: zaxchem@126.com (Ai-Xin Zhu) and huangbo15@foxmail.com (Bo Huang);.
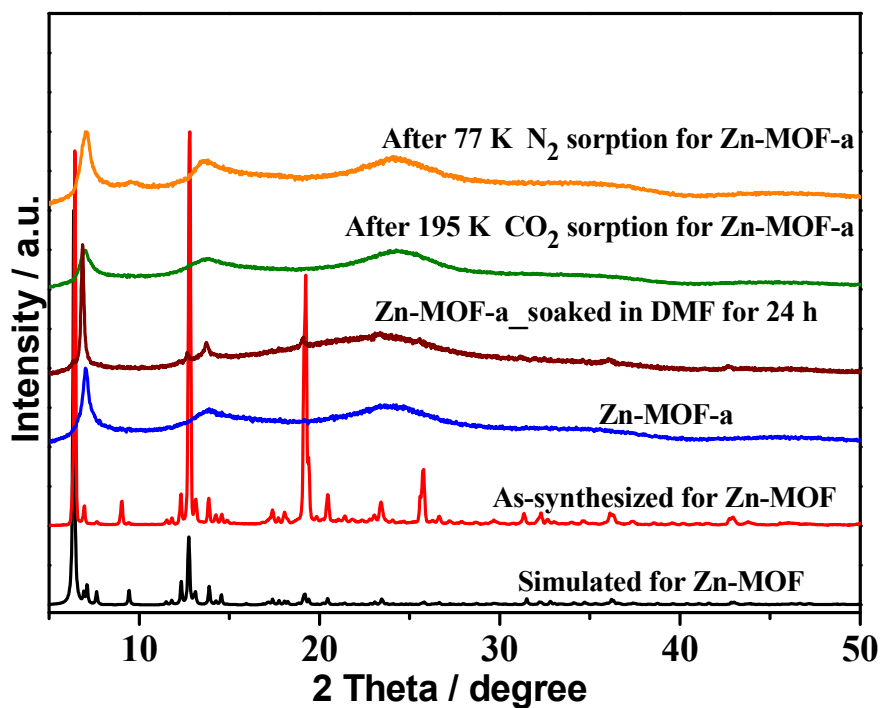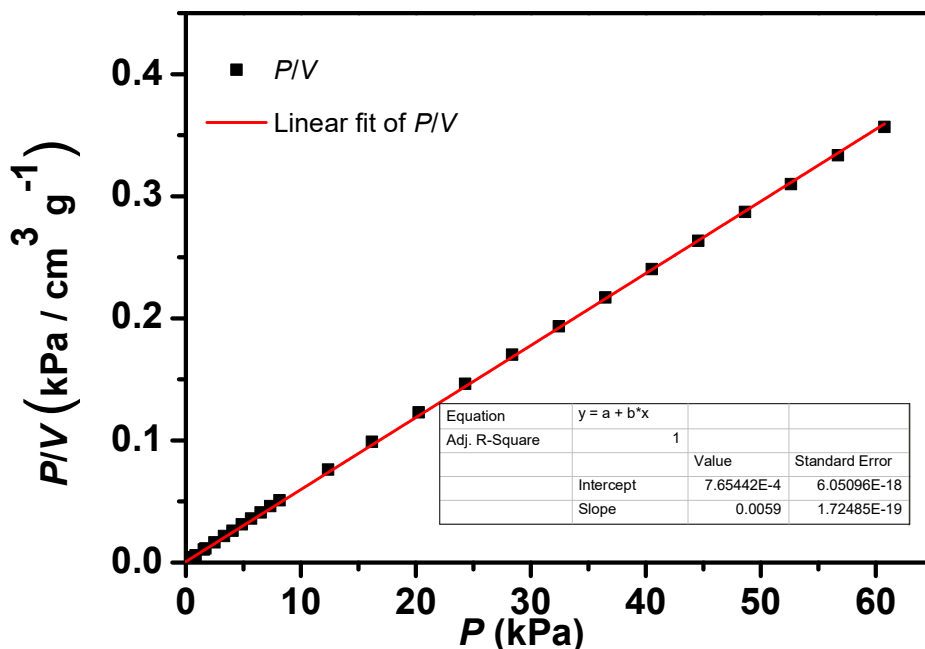
Fig. S1 PXRD patterns of **Zn-MOF**, **Zn-MOF-a**, **Zn-MOF-a** after being soaked in DMF for 24 h, and **Zn-MOF-a** after sorption of N_2 at 77 K and CO_2 at 195 K.
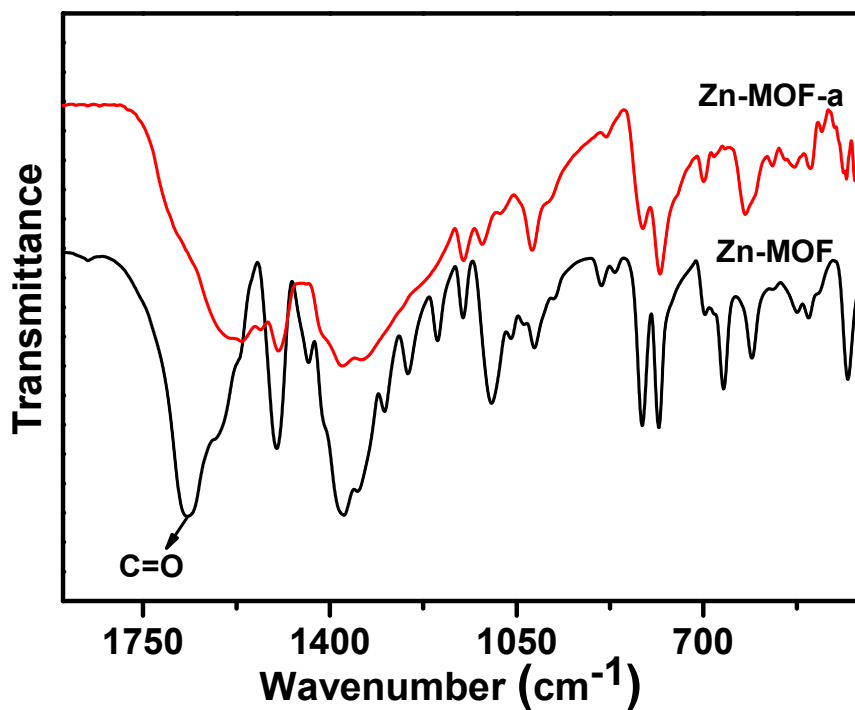
Fig. S2 FT-IR spectra of **Zn-MOF** and **Zn-MOF-a**. The lack of C=O stretching peaks at about 1668 cm^{-1} in the IR spectra of **Zn-MOF-a** confirms the full release of DMF guests.

The calculation of Langmuir surface area

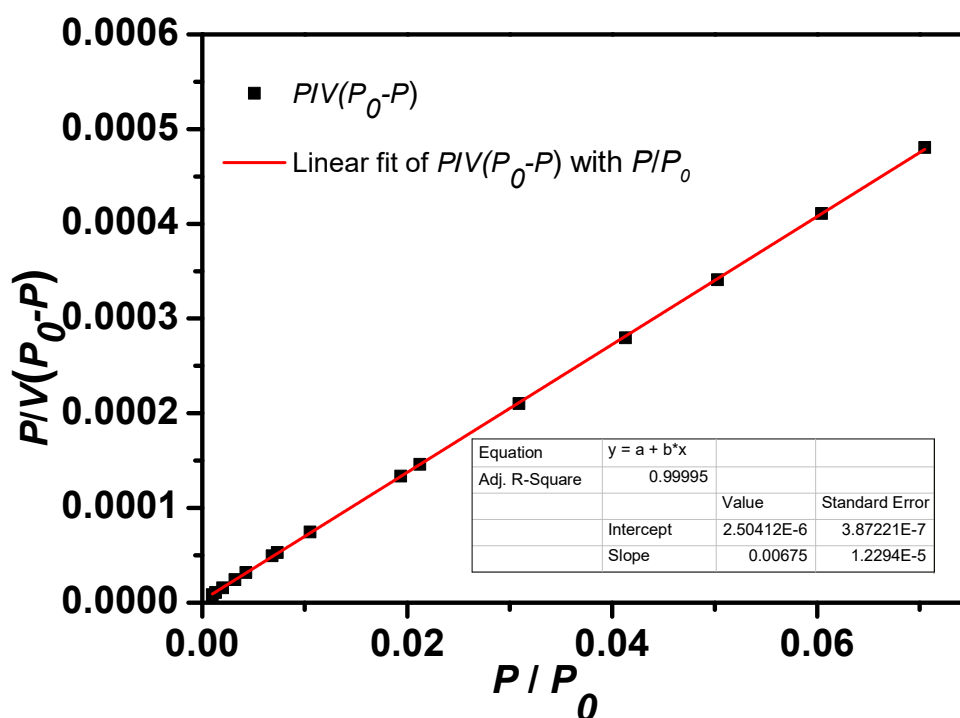| Equation	y = a + b*x		
Adj. R-Square	1		
		Value	Standard Error
	Intercept	7.65442E-4	6.05096E-18
	Slope	0.0059	1.72485E-19

Fig. S3 Langmuir plot for the N_2 adsorption isotherm of **Zn-MOF-a** at 77 K, and the range P from 0.0001125 to 60.75 KPa satisfies for applying the Langmuir theory.

The adsorption isotherms were converted into plots of P/V vs. P for determining the appropriate range. As shown in Fig. S3, the range P from 0.0001125 to 60.75 KPa satisfies for applying the Langmuir theory. After having identified the appropriate low pressure Langmuir P range, the analysis proceeds according to the standard method via the linearized Langmuir equation.

$$P/V = P/\,V_m + 1/BV_m$$

from which the parameters V_m is obtained from the relation $V_m = 1/s$, s being the slope with the ordinate of the plot P/V vs. P. The surface area is then obtained from $A_{Langmuir} = V_m\sigma_m N_A$ with σ_m being the cross-sectional area of N_2 at liquid density (16.25×10^{-20} m^2), and N_A Avogadro's number (6.023×10^{23}).

The calculation of BET surface area

Equation	y = a + b*x		
Adj. R-Square	0.99995		
		Value	Standard Error
	Intercept	2.50412E-6	3.87221E-7
	Slope	0.00675	1.2294E-5

Fig. S4 BET plot for the N_2 adsorption isotherm of **Zn-MOF-a** at 77 K, and the range P/P_0 from 0.055 to 0.204 satisfies for applying the BET theory.

The adsorption isotherms were converted into plots of $1/[V(P_0/P - 1)]$ vs. P/P_0 for determining the appropriate range. As shown in Fig. S4, the range P/P_0 from 0.0035 to 0.04 satisfies for applying the BET theory. After having identified the appropriate low pressure BET P/P_0 range, the analysis proceeds according to the standard method via the linearized BET equation.

$$\frac{P}{V(P_0 - P)} = \frac{1}{V_m c} + \frac{(C-1)}{V_m c}\frac{P}{P_0}$$

from which the BET parameters c is obtained from the relation $c = s/i + 1$, s being the slope and i being the intercept with the ordinate of the plot $1/[V(P_0/P - 1)]$ vs. P/P_0. The parameter V_m is then given by $V_m = 1/(s + i)$. The surface area is then obtained from $A_{BET} = V_m \sigma_m N_A$ with σ_m being the cross-sectional area of N_2 at liquid density (16.25×10^{-20} m^2), and N_A Avogadro's number (6.023×10^{23}).

Calculation of enthalpy of adsorption (Q_{st}) for CO_2

$$\ln P = \ln N + \sum_{i=0}^{m} a_i N^i + \sum_{i=0}^{n} \binom{n}{k} b_i N^i$$

$$Q_{st} = -R \sum_{i=0}^{m} a_i N^i$$

A virial-type expression of the above form was used to fit the combined isotherm data of CO_2 for **Zn-MOF-a** at 273, 283 and 298 K, where P is the pressure described in Pa, N is the adsorbed amount in mmol/g, T is the temperature in K, ai and bi are virial coefficients, and m and n are the number of coefficients used to describe the isotherms. Qst is the coverage-dependent enthalpy of adsorption and R is the universal gas constant.
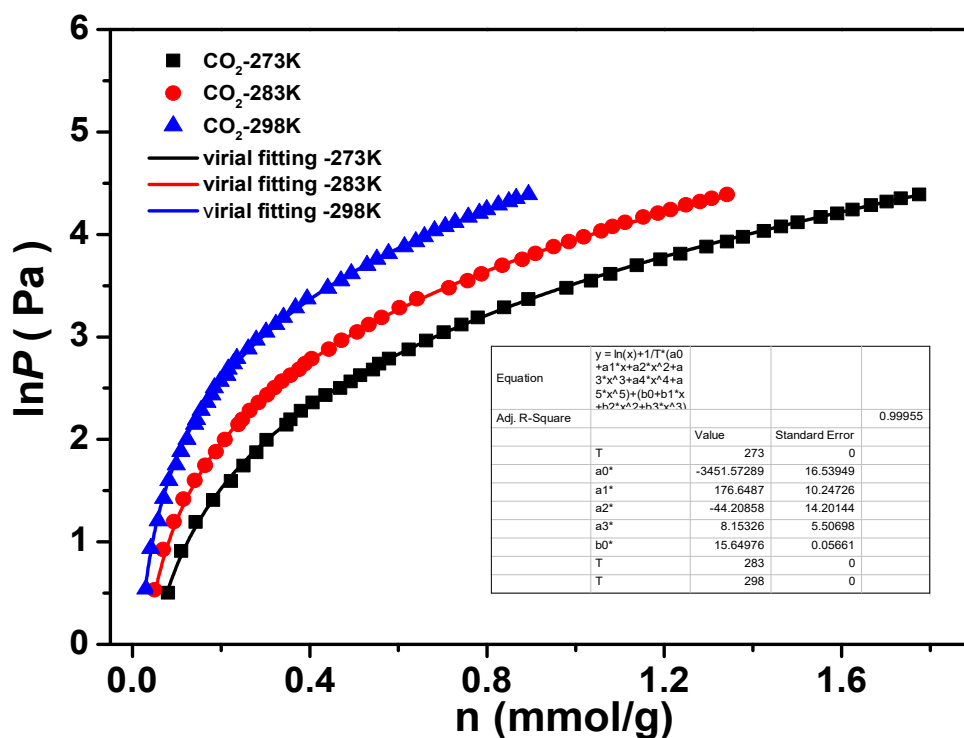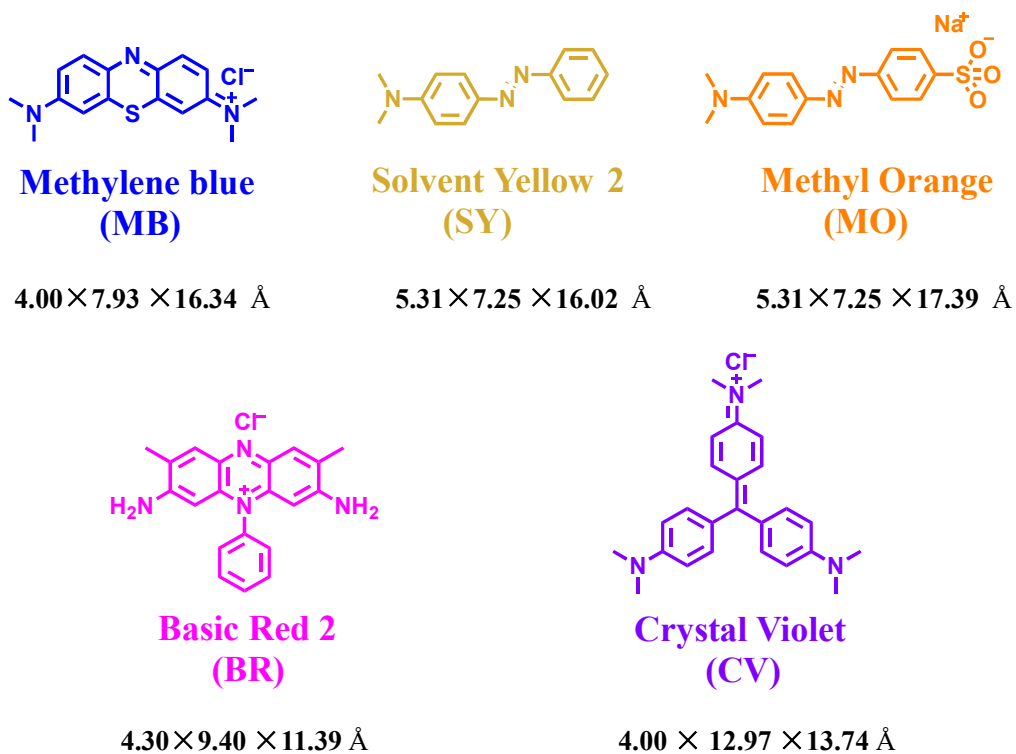

Equation	$y = \ln(x)+1/T*(a0 +a1*x+a2*x^2+a 3*x^3+a4*x^4+a 5*x^5)+(b0+b1*x +b2*x^2+b3*x^3)$		
Adj. R-Square			0.99955
		Value	Standard Error
	T	273	0
	a0*	-3451.57289	16.53949
	a1*	176.6487	10.24726
	a2*	-44.20858	14.20144
	a3*	8.15326	5.50698
	b0*	15.64976	0.05661
	T	283	0
	T	298	0

Fig. S5 The virial fitting of CO_2 sorption data for **Zn-MOF-a**.

Methylene blue (MB)

$4.00 \times 7.93 \times 16.34$ Å

Solvent Yellow 2 (SY)

$5.31 \times 7.25 \times 16.02$ Å

Methyl Orange (MO)

$5.31 \times 7.25 \times 17.39$ Å

Basic Red 2 (BR)

$4.30 \times 9.40 \times 11.39$ Å

Crystal Violet (CV)

$4.00 \times 12.97 \times 13.74$ Å

Scheme S1 Chemical Structures of five organic dyes with different charge and size.
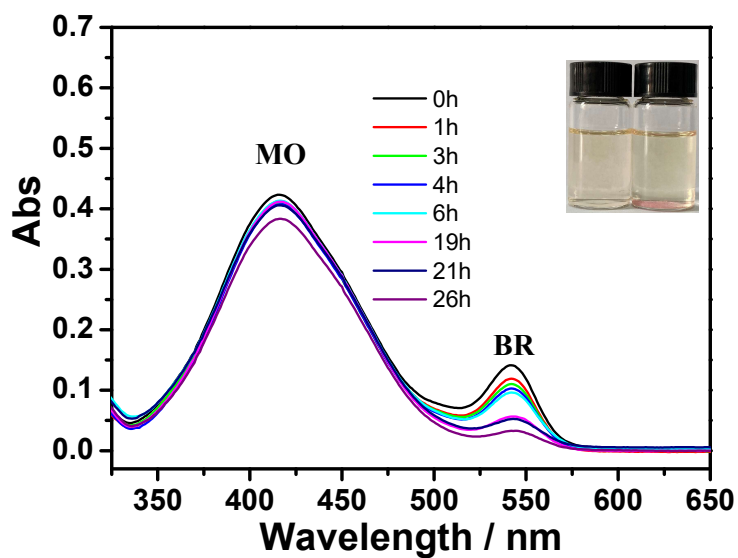
Fig. S6 Selective adsorption capability of mixed dyes MO & BR for **Zn-MOF**.
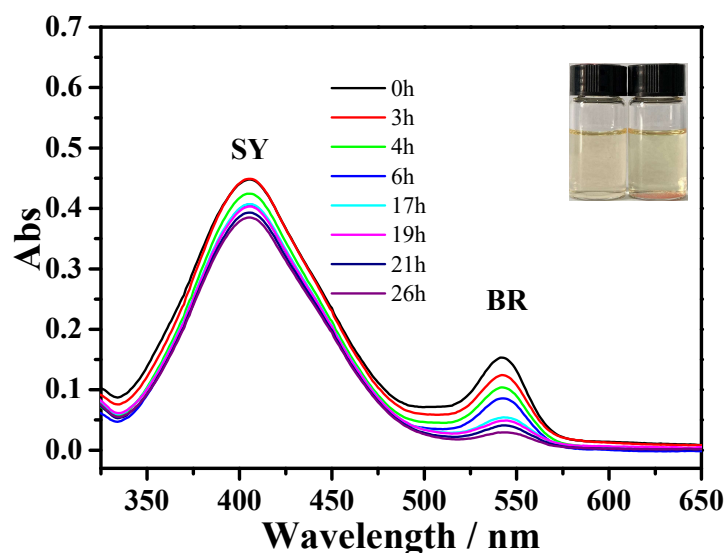
Fig. S7 Selective adsorption capability of mixed dyes SY & BR for **Zn-MOF**.

Reusability experiment for dyes adsorption

For each cycle of dyes adsorption, the samples (20 mg) were added to a 4 mL EtOH solution of each cationic dyes (1.0×10^{-5} mol·L^{-1}), and the UV-vis spectra of the solution were collected at room temperature before and after the crystals of **Zn-MOF** addition for 26 h to check the recyclable and reusable ability. After each cycle of dyes adsorption, the regeneration of **Zn-MOF** was achieved by the following procedure: the dye-adsorbed samples (**dye@Zn-MOF**) were soaked in a saturated EtOH solution of LiCl for 30 min, the solution were replaced with a new saturated EtOH solution of LiCl for several times until the solution has no color change, and then the sample were filtered and dry at room temperature.
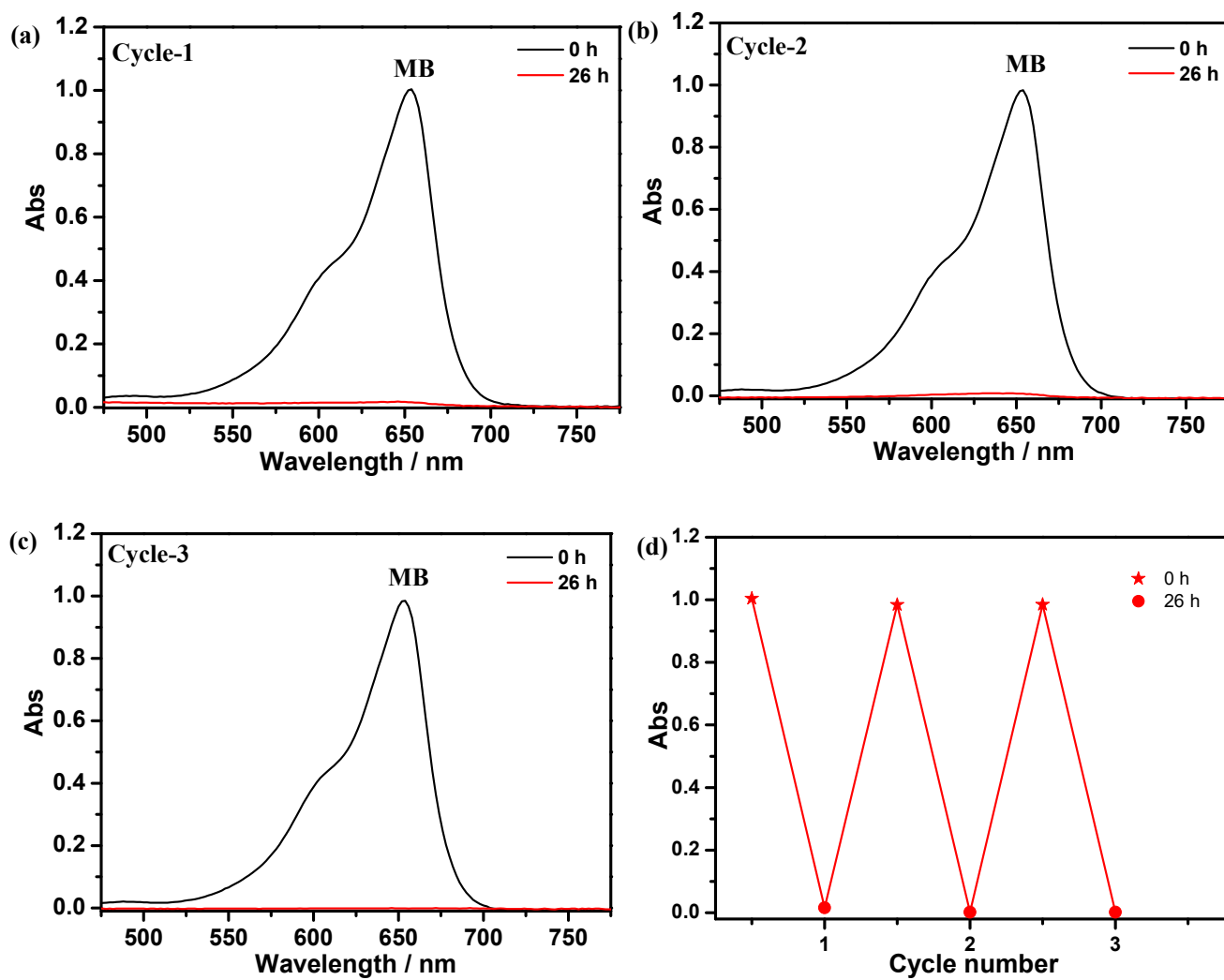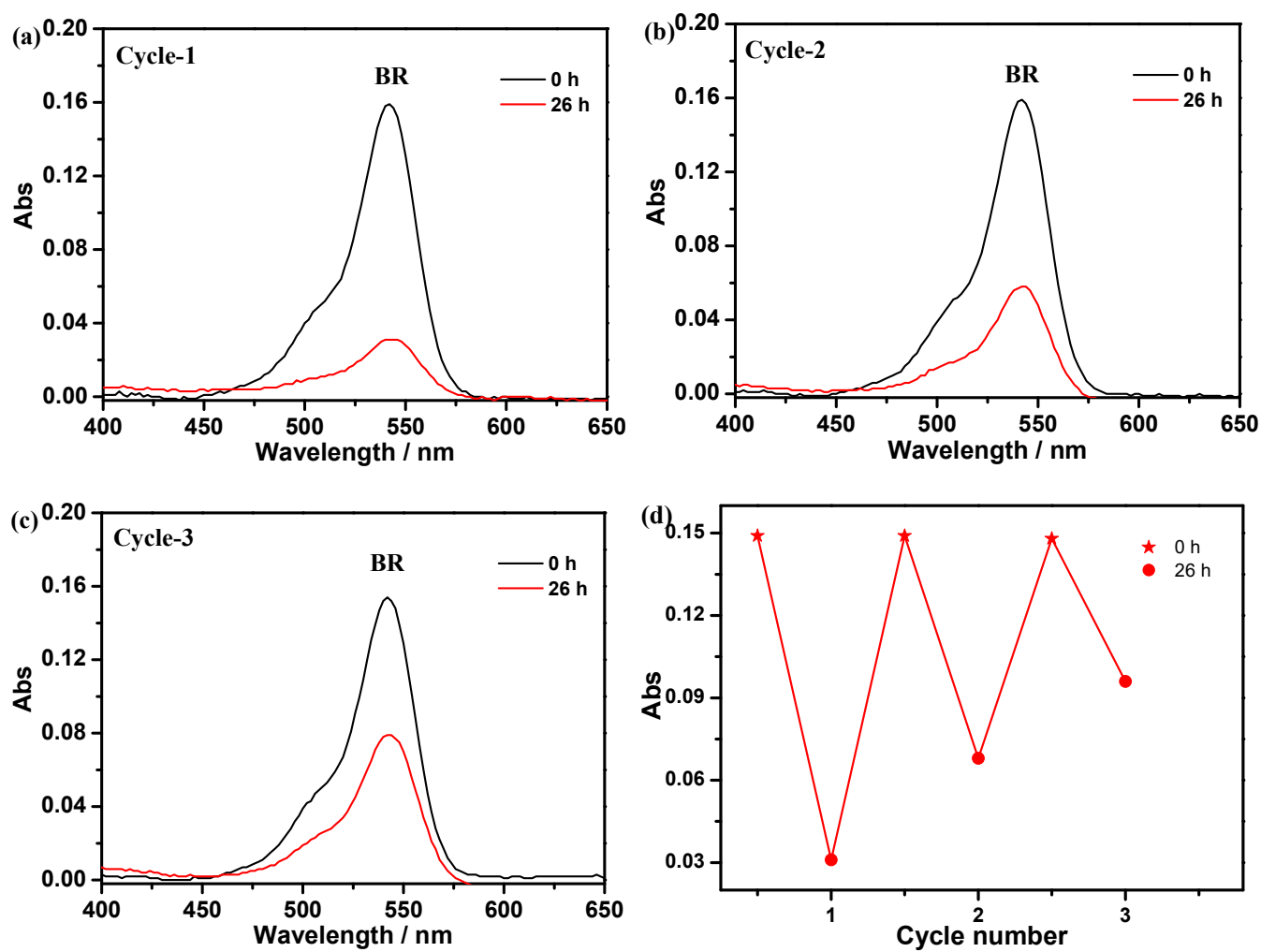
Fig. S8 The three cycles of MB absorption by **Zn-MOF**. (a) the first cycle of MB absorption; (b) the second cycle of MB absorption; (c) the third cycle of MB absorption; (d) the adsorption ability of 3 cycles of MB adsorption.
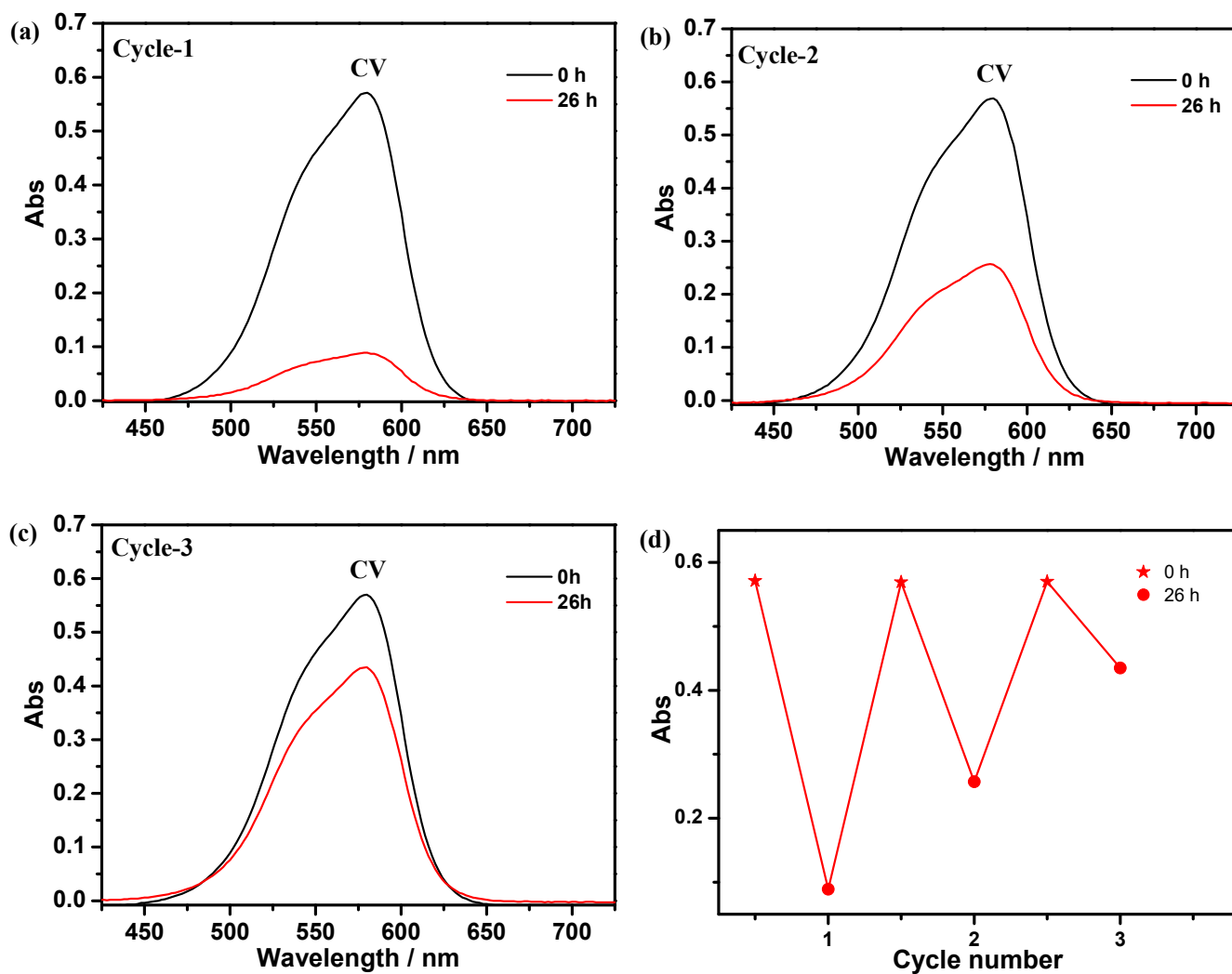
Fig. S9 The three cycles of CV absorption by **Zn-MOF**. (a) the first cycle of CV absorption; (b) the second cycle of MB absorption; (c) the third cycle of CV absorption; (d) the adsorption ability of 3 cycles of CV adsorption.

Fig. S10 The three cycles of BR absorption by **Zn-MOF**. (a) the first cycle of BR absorption; (b) the second cycle of MB absorption; (c) the third cycle of BR absorption; (d) the adsorption ability of 3 cycles of BR adsorption.
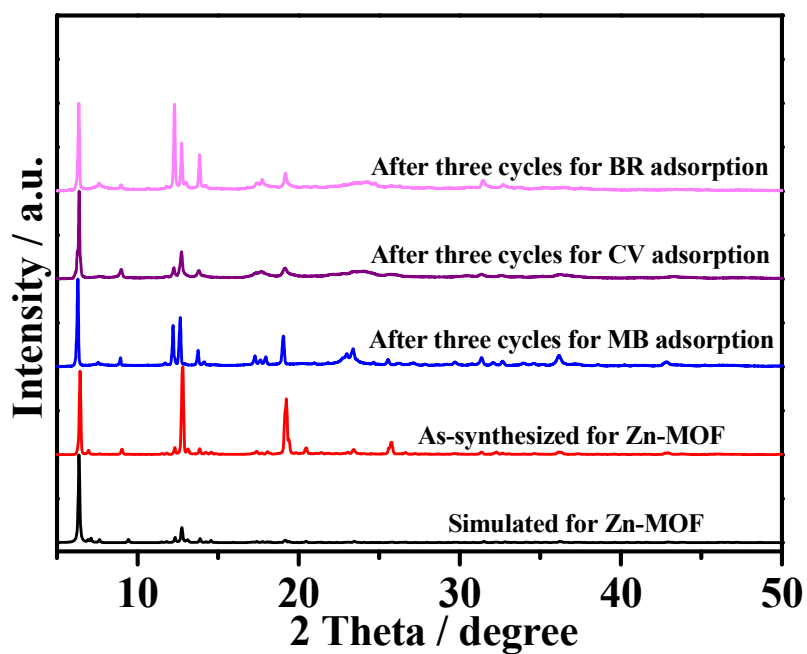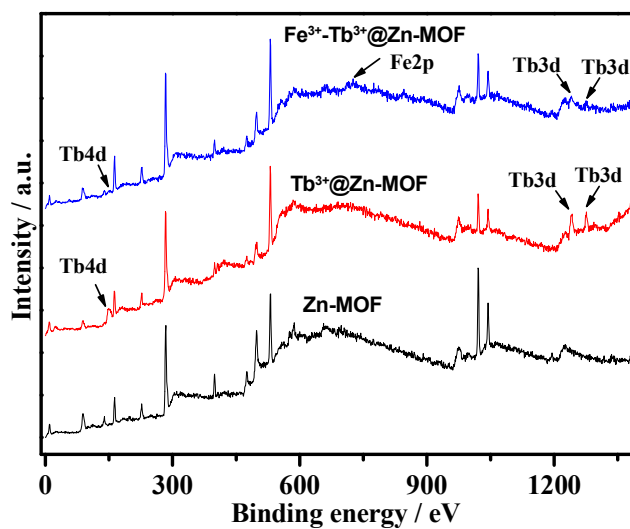
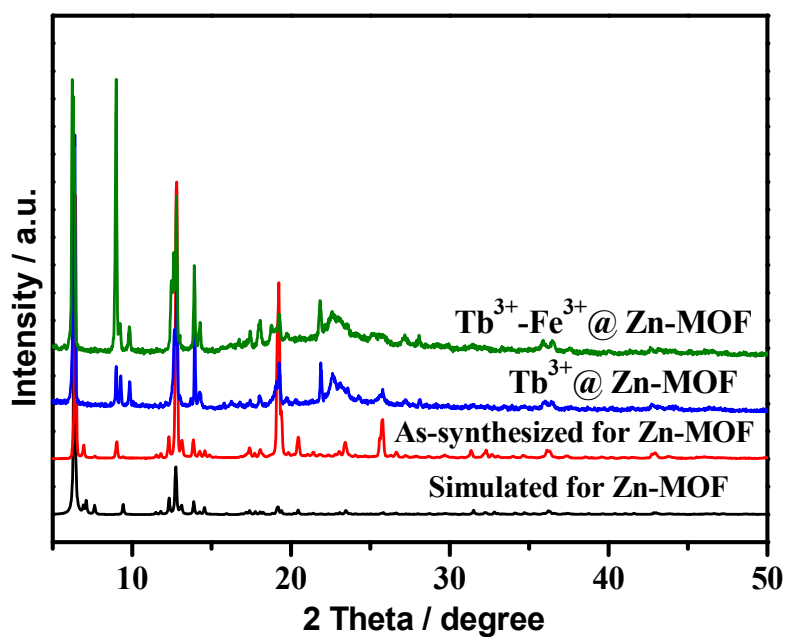**Fig. S11** PXRD patterns of **Zn-MOF** after three cycles of dyes adsorption.
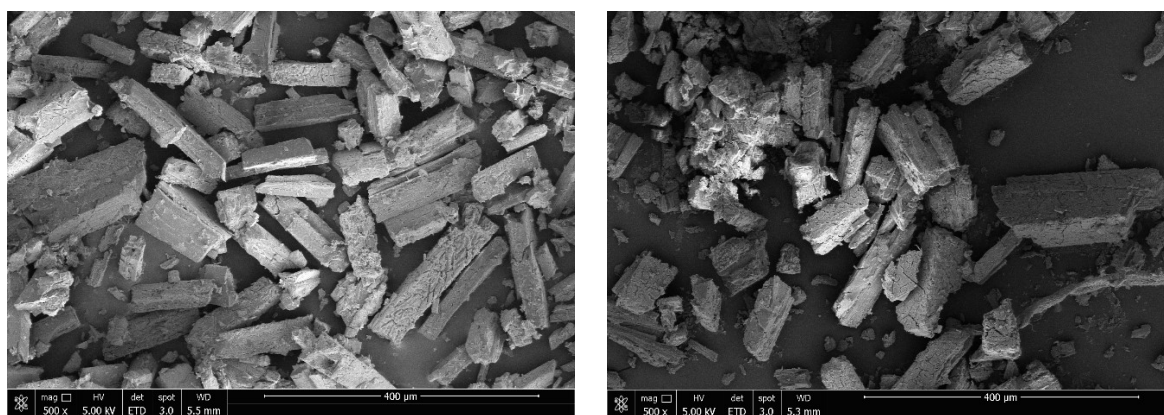
Fig. S12 (a) SEM image of Tb^{3+}@**Zn-MOF**. (b) SEM image of Tb^{3+}@**Zn-MOF** after being soaking in EtOH solution of $Fe(NO_3)_3$ for 12 h.
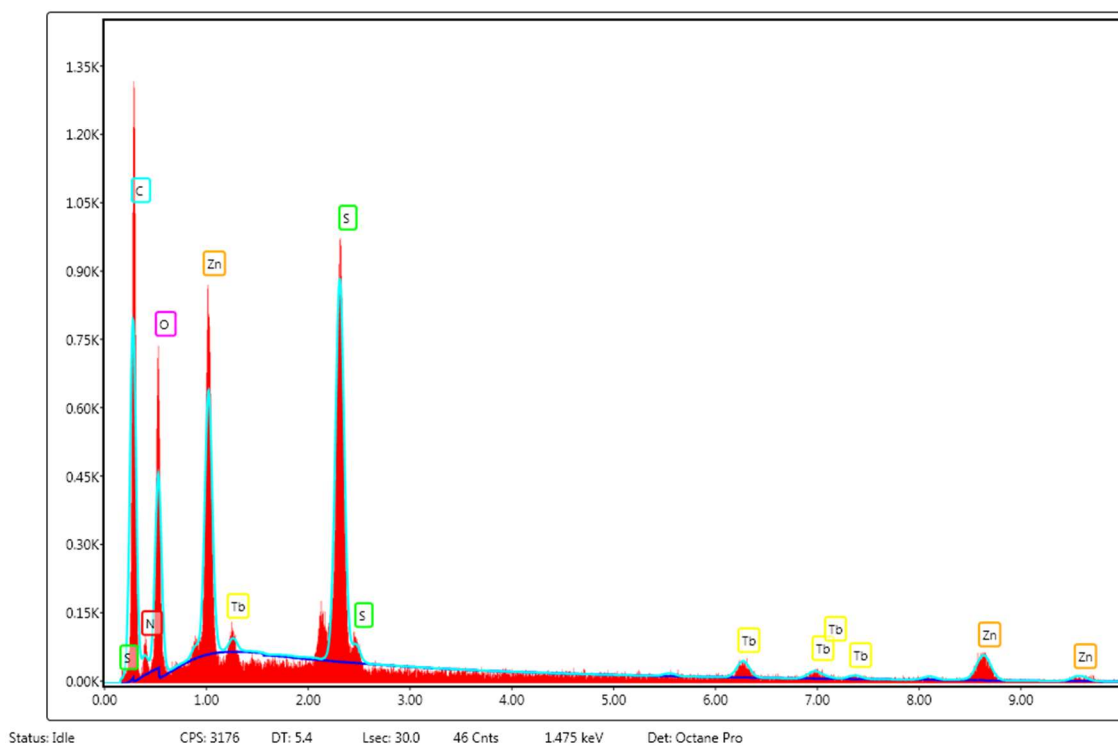
Fig. S13 The SEM-EDS analysis for Tb^{3+}@**Zn-MOF**.

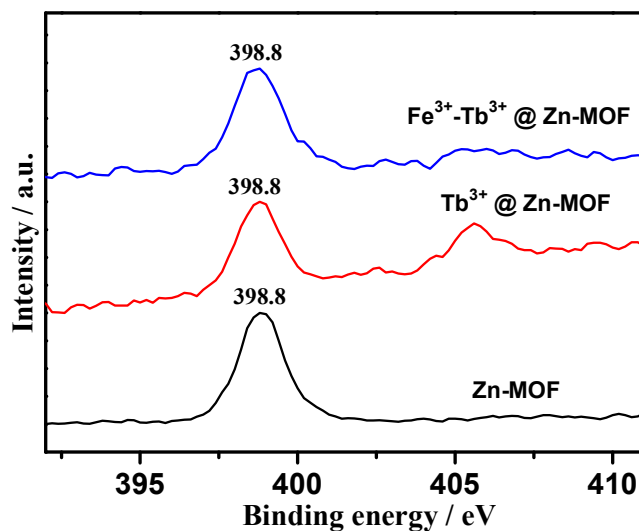**Fig. S14** XPS low-resolution survey scan of **Zn-MOF**, Tb^{3+}@**Zn-MOF** and the sample of Tb^{3+}@**Zn-MOF** after Fe^{3+} addition.
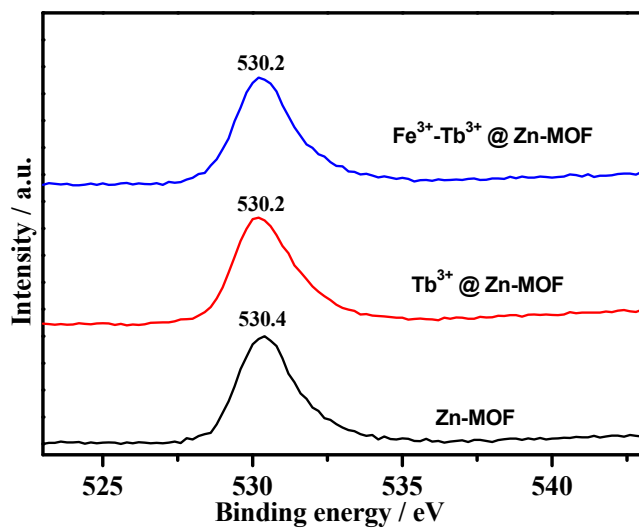
Fig. S15 PXRD patterns of for **Zn-MOF**, Tb^{3+}@**Zn-MOF** and the sample of Tb^{3+}@**Zn-MOF** after being soaking in EtOH solution of $Fe(NO_3)_3$ for 12 h.
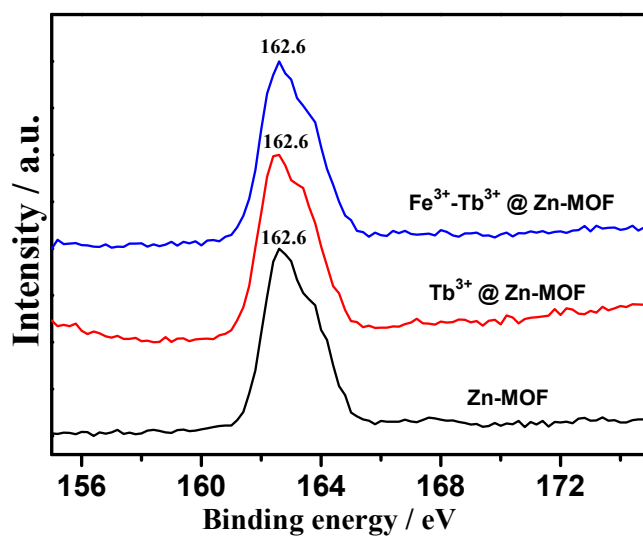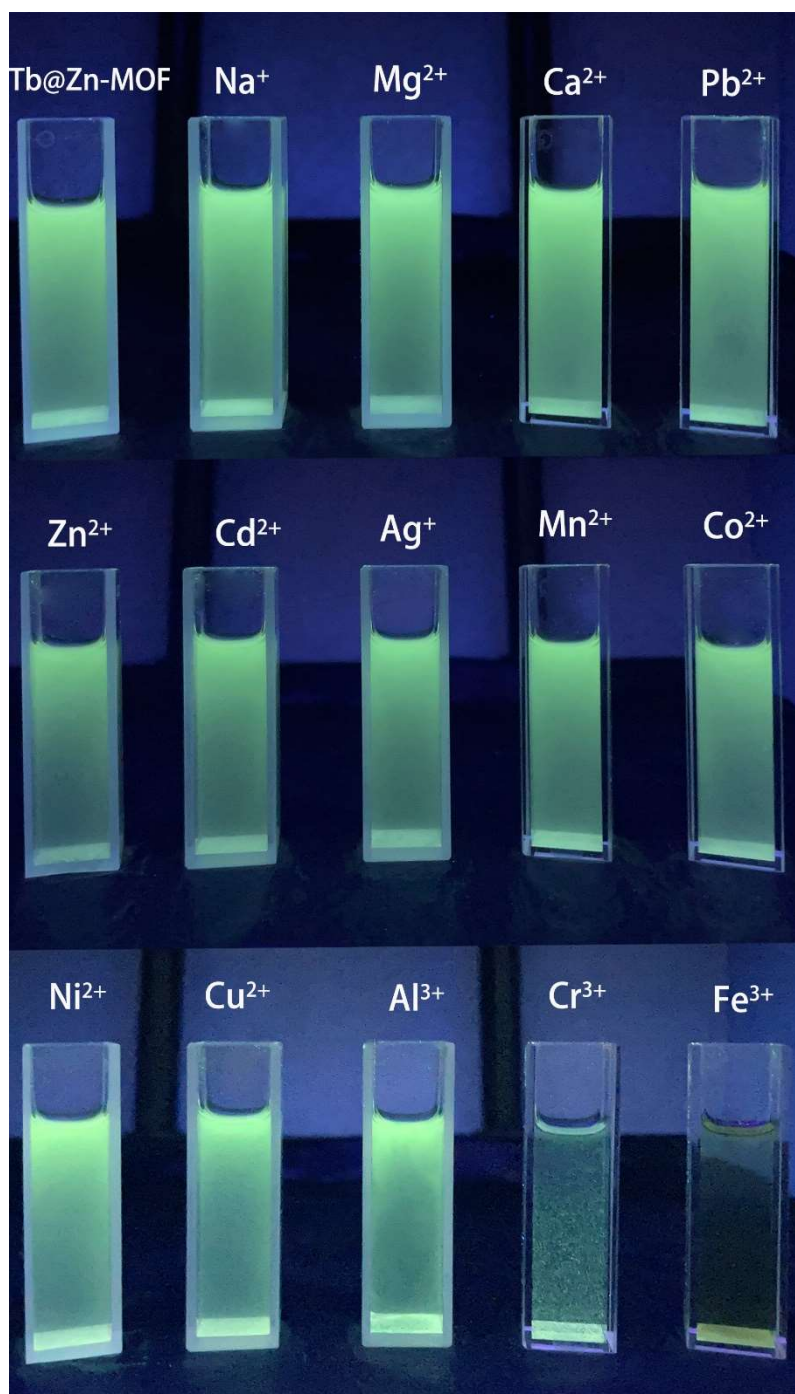

Fig. S16 XPS high-resolution survey scans of S2p for **Zn-MOF**, Tb^{3+}@**Zn-MOF** and the sample of Tb^{3+}@**Zn-MOF** after Fe^{3+} sensing.

Fig. S17 XPS high-resolution survey scans of N1s for **Zn-MOF**, Tb^{3+}@**Zn-MOF** and the sample of Tb^{3+}@**Zn-MOF** after Fe^{3+} sensing.
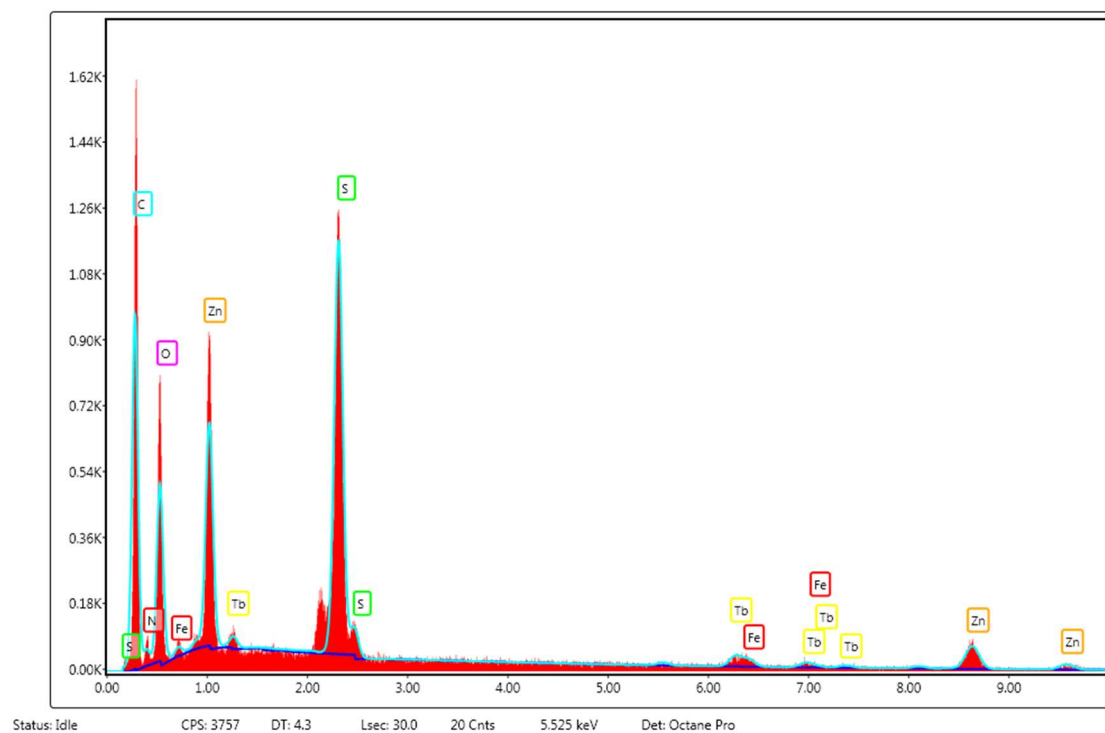

Fig. S18 XPS high-resolution survey scans of O1s for **Zn-MOF**, Tb^{3+}@**Zn-MOF** and the sample of Tb^{3+}@**Zn-MOF** after Fe^{3+} sensing.

Fig. S19 The photograph of Tb^{3+}@**Zn-MOF** dispersed in EtOH with the addition of different metal ions under UV irradiation.

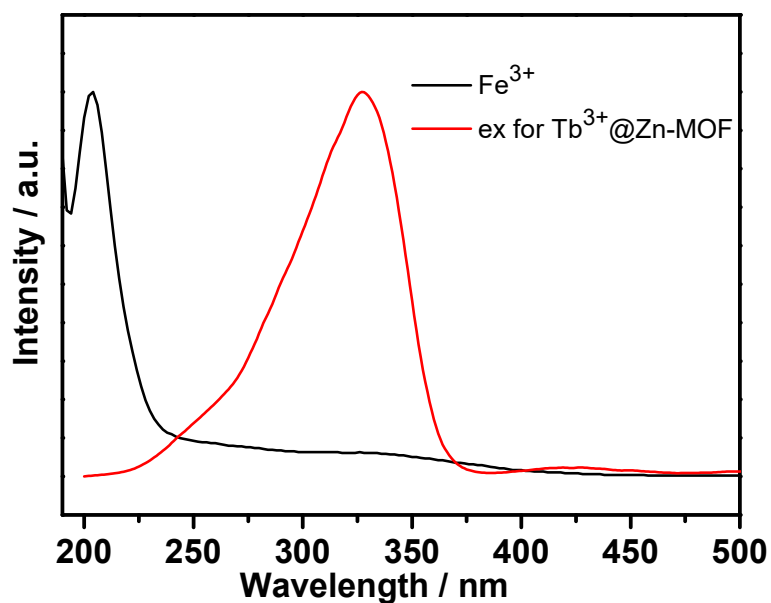**Fig. S20** The SEM-EDS analysis for Tb^{3+}@**Zn-MOF** after being soaking in EtOH solution of Fe(NO$_3$)$_3$.

Fig. S21 The photographs of **Zn-MOF**, Tb^{3+}@**Zn-MOF** and Fe^{3+}-incorporated Tb^{3+}@**Zn-MOF**.

Fig. S22 The excitation spectra of Tb^{3+}@**Zn-MOF** (dispersed in EtOH) and Uv-vis absorption spectrum of $Fe(NO_3)_3$ in EtOH.

Table S1 Summary of isosteric heat of adsorption (Q_{st}) of CO_2 for anionic metal-organic frameworks

Compound	Using methods	Q_{st} / KJ·mol^{-1}	Ref
$H_3[(Cu_4Cl)_3(BTTri)_8]$	Clausius-Clapeyron equation	21.0	1
SNU-151'	Clausius-Clapeyron equation	27.1	2
FJI-C1	virial methods	20.7	3
$[H_2N(Me)_2]_2[Zn_5(L)_3]$	virial methods	23.0	4
ZJNU-55a	Clausius-Clapeyron equation	35.4	5
CPF-13	virial methods	28.2	6
JXNU-4	virial methods	27.8	7
Bio-MOF-1	Clausius-Clapeyron equation	35.0	8
$[(CH_3)_2NH_2]_3[Zn_4Na(BPTC)_3]$	Clausius–Clapeyron equation	27.0	9
$\{[NH_2(CH_3)_2][Zn(atz)(ox)]\cdot H_2O\}_n$	Clausius–Clapeyron equation	45.4	10
$\{(Me_2NH_2)[Co_3(OH)_2(TCPP)_2(bpy)](DMF)_{15}\}_n$	virial methods	23.5	11

Table S2 The comparison among anionic metal-organic frameworks used for sensing Fe^{3+}

Fluorescent materials	Media (aqueous / organic)	Quenching constant K_{sv} (M^{-1})	LOD(limit of detection) (M)	Ref.
Tb^{3+}@Zn-MOF	EtOH	3.26×10^4	1.67×10^{-6}	this work
$[(CH_3)_2NH_2]\cdot[Tb(bptc)]\cdot xsolvents$	EtOH	/	1.8×10^{-4}	12
$[CH_3\text{-}dpb]_2[Mg_3(1,4\text{-}NDC)_4(\mu\text{-}H_2O)_2(CH_3OH)(H_2O)]\cdot 1.5H_2O$	EtOH	1.6×10^4	4.7×10^{-4}	13
Eu^{3+}@bio-MOF-1	H_2O	3.38×10^3	/	14
$\{[(CH_3)_2NH_2]_4[Ca_2Zn_4(L)_4]\cdot 4DMF\}_n$	H_2O	4.36×10^3	1.88×10^{-5}	15
$[H_2N(CH_3)_2]_2[Zn_2L(HPO_3)_2]$	H_2O	3.96×10^5	1.16×10^{-4}	16
$[H_2N(CH_3)_2]_3[Tb(dipic)_3]$	H_2O	3.60×10^4	/	17
$[H_2N(Me)_2][Eu_3(OH)(bpt)_3(H_2O)_3]$ $(DMF)_2\cdot(H_2O)_4$	H_2O	3.27×10^4	/	18
$[(CH_3)_2NH_2]_6[Cd_3L(H_2O)_2]\cdot 12H_2O$	H_2O	2.67×10^5	/	19
$\{(Me_2NH_2)[Eu_3(PTTBA)_2]\cdot xDMF\cdot yH_2O\}_n$	H_2O	4.75×10^4	6.32×10^{-6}	20
$[Me_2NH_2][Eu(CPA)_2(H_2O)_2]$	H_2O	1.04×10^4	1×10^{-7}	21
NUC-7	H_2O	4.77×10^4	6.3×10^{-6}	22
$[(CH_3)_2NH_2]_2[Tb_2(L)_2(H_2O)_2]\cdot 2DMF\cdot 2H_2O$	H_2O	7.58×10^4	5×10^{-5}	23
$\{(Me_2NH_2)[Zn_2(L)(H_2O)]\cdot 0.5DMF\}_n$	DMF	7.83×10^3	1.45×10^{-5}	24
FJI-C8	DMF	8.245×10^3	2.33×10^{-5}	25
$\{(NC_2H_8)_2[Cd(DMIPA)]\cdot xG\}_n$	DMF	3.78×10^4	2.9×10^{-5}	26
JOU-23	DMF	5.98×10^4	2×10^{-6}	27
JOU-11	DMF	2.66×10^4	4.53×10^{-6}	28
$[H_2N(CH_3)_2][Cd_4(Hdpa)_2(DMA)_2(H_2O)_3]\cdot 1.5DMA\cdot 2H_2O$	DMF	3.77×10^4	/	29
$\{[Cd_2(L)(DMA)]\cdot[H_2N(Me)_2]\}_n$	DMA	4.90×10^3	1.2×10^{-3}	30
$[Eu(BTEC)_{0.5}(HCOO)(H_2O)_2]$	DMSO	3.19×10^4	/	31

References:

1. A. Demessence, D. M. D'Alessandro, M. L. Foo and J. R. Long, *J. Am. Chem. Soc.*, 2009, **131**, 8784-8786.
2. M. H. Choi, H. J. Park, D. H. Hong and M. P. Suh, *Chem. Eur. J.*, 2013, **19**, 17432-17438.
3. Y. B. Huang, Z. J. Lin, H. R. Fu, F. Wang, M. Shen, X. S. Wang and R. Cao, *ChemSusChem*, 2014, **7**, 2647-2653.
4. B. Liu, R. Zhang, C. Y. Pan and H. L. Jiang, *Inorg. Chem.*, 2017, **56**, 4263-4266.
5. J. J. Jiao, H. M. Liu, F. L. Chen, D. J. Bai, S. S. Xiong and Y. B. He, *Inorg. Chem. Front.*, 2016, **3**, 1411-1418.
6. Q. G. Zhai, Q. Lin, T. Wu, L. Wang, S. T. Zheng, X. H. Bu and P. Y. Feng, *Chem. Mater.*, 2012, **24**, 2624-2626.
7. H. F. Ma, Q. Y. Liu, Y. L. Wang and S. G. Yin, *Inorg. Chem.*, 2017, **56**, 2919-2925.
8. J. An and N. L. Rosi, *J. Am. Chem. Soc.*, **132**, 5578-5579.
9. E. L. Zhou, P. Huang, C. Qin, K. Z. Shao and Z. M. Su, *J. Mater. Chem. A*, 2015, **3**, 7224-7228.
10. R. Y. Chen, D. Tian, Y. W. Li, Y. B. Lv, H. W. Sun, Z. Chang and X. H. Bu, *RSC Adv.*, 2015, **5**, 24655-24660.
11. G. Ye, L. Chen, X. X. Yin, D. L. Liu, M. N. Wang, Q. F. Zhang, Y. Liu, W. Liu and H. Y. Zhang, *Sep. Sci. Technol.*, 2020, **56**, 36-44.
12. X. L. Zhao, D. Tian, Q. Gao, H. W. Sun, J. Xu and X. H. Bu, *Dalton Trans.*, 2016, **45**, 1040-1046.
13. Z. F. Wu, L. K. Gong and X. Y. Huang, *Inorg. Chem.*, 2017, **56**, 7397-7403.
14. X. Shen and B. Yan, *J. Colloid Interface Sci.*, 2015, **451**, 63-68.

15. W. J. Ji, G. F. Liu, B. Q. Wang, W. B. Lu and Q. G. Zhai, *CrystEngComm*, 2020, **22**, 4710-4715.
16. S. F. Tang and X. M. Hou, *Cryst. Growth Des.*, 2018, **19**, 45-48.
17. H. B. Zhang, P. Hu, Q. K. Zhang, M. D. Huang, C. Z. Lu, V. Malgras, Y. Yamauchi, J. Zhang and S. W. Du, *Chem. Eur. J.*, 2015, **21**, 11767-11772.
18. S. H. Xing, Q. M. Bing, L. F. Song, G. H. Li, J. Y. Liu, Z. Shi, S. H. Feng and R. R. Xu, *Chem. Eur. J.*, 2016, **22**, 16230-16235.
19. B. B. Lu, W. Jiang, J. Yang, Y. Y. Liu and J. F. Ma, *ACS Appl. Mater. Interfaces*, 2017, **9**, 39441-39449.
20. H. T. Chen, L. M. Fan, H. X. Lv and X. T. Zhang, *Inorg. Chem.*, 2020, **59**, 13407-13415.
21. Y. P. Wu, G. W. Xu, W. W. Dong, J. Zhao, D. S. Li, J. Zhang and X. H. Bu, *Inorg. Chem.*, 2017, **56**, 1402-1411.
22. H. T. Chen, L. M. Fan and X. T. Zhang, *ACS Appl. Nano Mater.*, 2020, **3**, 7201-7210.
23. J. J. Huang, J. H. Yu, F. Q. Bai and J. Q. Xu, *Cryst. Growth Des.*, 2018, **18**, 5353-5364.
24. J. Wang, X. R. Wu, J. Q. Liu, B. H. Li, A. Singh, A. Kumar and S. R. Batten, *CrystEngComm*, 2017, **19**, 3519-3525.
25. C. H. Chen, X. S. Wang, L. Li, Y. B. Huang and R. Cao, *Dalton Trans.*, 2018, **47**, 3452-3458.
26. T. Gao, B. X. Dong, Y. M. Pan, W. L. Liu and Y. L. Teng, *J. Solid State Chem.*, 2019, **270**, 493-499.
27. H. Zhang, J. Wu, W. Y. Geng, Y. H. Luo, Z. J. Ding, Z. X. Wang and D. E. Zhang, *J. Solid State Chem.*, 2021, **302**, 122424.
28. Y. H. Luo, A. D. Xie, M. G. Hu, J. Wu, D. E. Zhang and Y. Q. Lan, *Inorg. Chem.*, 2021, **60**, 167-174.
29. J. C. Jin, L. Y. Pang, G. P. Yang, L. Hou and Y. Y. Wang, *Dalton Trans.*, 2015, **44**, 17222-17228.
30. Y. T. Yan, J. Liu, G. P. Yang, F. Zhang, Y. K. Fan, W. Y. Zhang and Y. Y. Wang, *CrystEngComm*, 2018, **20**, 477-486.
31. Y. W. Shi, J. W. Ye, Y. Qi, M. A. Akram, A. Rauf and G. L. Ning, *Dalton Trans.*, 2018, **47**, 17479-17485.